WHITE NOISE ANALYSIS OF *PHYCOMYCES* LIGHT GROWTH RESPONSE SYSTEM

I. NORMAL INTENSITY RANGE

E. D. LIPSON

From the Division of Biology, California Institute of Technology, Pasadena, California 91125

ABSTRACT The Wiener-Lee-Schetzen method for the identification of a nonlinear system through white gaussian noise stimulation was applied to the transient light growth response of the sporangiophore of *Phycomyces*. In order to cover a moderate dynamic range of light intensity I, the input variable was defined to be log I. The experiments were performed in the normal range of light intensity, centered about $I_0 = 10^{-6}$ W/cm^2. The kernels of the Wiener functionals were computed up to second order. Within the range of a few decades the system is reasonably linear with log I. The main nonlinear feature of the second-order kernel corresponds to the property of rectification. Power spectral analysis reveals that the slow dynamics of the system are of at least fifth order. The system can be represented approximately by a linear transfer function, including a first-order high-pass (adaptation) filter with a 4 min time constant and an underdamped fourth-order low-pass filter. Accordingly a linear electronic circuit was constructed to simulate the small scale response characteristics. In terms of the adaptation model of Delbrück and Reichardt (1956, in *Cellular Mechanisms in Differentiation and Growth*, Princeton University Press), kernels were deduced for the dynamic dependence of the growth velocity (output) on the "subjective intensity," a presumed internal variable. Finally the linear electronic simulator above was generalized to accommodate the large scale nonlinearity of the adaptation model and to serve as a tool for deeper tests of the model.

INTRODUCTION

The growth velocity of *Phycomyces* sporangiophores can be modulated by varying the light intensity. Measurements of this light growth response using pulse, step, and sinusoidal light stimuli have been reported recently (Foster and Lipson, 1973). To characterize the light growth response system in a more efficient, compact, and meaningful fashion a new approach has been adopted, wherein "white noise" stimulus programs are used to derive the Wiener kernels of the system (Wiener, 1958; Lee and Schetzen, 1965). This method has been applied very effectively to retinal neural systems in the catfish (Marmarelis and Naka, 1973) and in the fly (McCann, 1974).

In contrast to these studies on multicellular neural pathways, this work is concerned with a stimulus-response pathway which starts and ends within a single cell. The first paper of this series presents a detailed analysis of the response in the "normal range"

of light intensity, as defined by Delbrück and Reichardt (1956). The second paper (Lipson, 1975*a*, referred to as paper II) treats the entire dynamic range of light intensities relevant for *Phycomyces*. The third paper (Lipson, 1975*b*, referred to as paper III) examines components of the stimulus-response pathway by analyzing representative photomutants.

Formalism of White Noise Analysis

Wiener (1958) first recognized that a nonlinear system could be identified by analyzing its response to white gaussian noise, provided only that the system exhibited time-invariance, boundedness, and finite memory. For such a system with white gaussian noise input $x(t)$ and output $y(t)$, he showed that the output could be decomposed into a sum of orthogonal "G-functionals,"

$$y(t) = \sum_{n=0}^{\infty} G_n[h_n, x(t)] \tag{1}$$

where the components G_n are linked to the input function by means of the series of kernels h_n:

$$G_0[h_0, x(t)] = h_0,$$

$$G_1[h_1, x(t)] = \int_{-\infty}^{\infty} h_1(\tau_1)x(t - \tau_1)\,d\tau_1,$$

$$G_2[h_2, x(t)] = \int_{-\infty}^{\infty}\int_{-\infty}^{\infty} h_2(\tau_1, \tau_2)x(t - \tau_1)x(t - \tau_2)\,d\tau_1\,d\tau_2 - K\int_{-\infty}^{\infty} h_2(\tau, \tau)\,d\tau,$$

and so on, where K is the power spectral density $\Phi_{xx}(f)$ of $x(t)$.

Lee and Schetzen (1965) devised a practical computational technique for determining the Wiener kernels h_n by means of a cross-correlation analysis between $x(t)$ and $y(t)$. Specifically,

$$h_n(\sigma_1, \sigma_2, \cdots, \sigma_n) = \frac{1}{n!K^n}\left\langle\left\{y(t) - \sum_{m=0}^{n-1} G_m[h_m, x(t)] \cdot x(t - \sigma_1)x(t - \sigma_2)\cdots x(t - \sigma_n)\right\}\right\rangle \tag{2}$$

where the angle brackets indicate an average over time t.

METHODS

Strain and Culture Conditions

The work in this paper is restricted to the albino mutant C2 (genotype *carA5*(−)), which shows photophysiology virtually identical to its parent wild-type *Phycomyces* strain

NRRL1555(−) (see end of paper III). The culture conditions were the same as in Foster and Lipson (1973).

Tracking Machine

All experiments were performed on the *Phycomyces* tracking machine (Foster and Lipson, 1973; Foster, 1972), which provides a continuous record of the vertical growth velocity of a single sporangiophore. The specimen was located in a temperature-controlled chamber at 20.5 ± 0.5°C. The machine maintained the light-sensitive growing zone, just beneath the sporangium, in a fixed position in the stimulating light beams. Bilateral oblique illumination at 30° above the horizontal was achieved by means of a beam splitter and mirror system. During experiments (duration about 6 h) the sporangiophore typically grew 2 cm from an initial length of 2 cm.

Light Source

In all experiments the light source was a Coherent Radiation Model 52G argon ion laser (Coherent Radiation, Palo Alto, Calif.). The laser was operated in light-regulation mode at a wavelength of 488 nm. The beam was expanded with a lens pair to a diameter of about 1 cm at the specimen.

Light Intensity Control and Calibration

To vary the light intensity dynamically, a 4.0 OD Inconel-coated circular neutral-density wedge was used (Kodak A-6040, Eastman Kodak Co., Rochester, N.Y.). The logarithm of the transmitted intensity was proportional to the wedge angle, and this angle was controlled by an electronic servo system. The absolute reference intensity level for each experiment was set by suitable combinations of neutral density filters and by adjustment of the laser intensity.

The wedge was calibrated with silicon photodiodes, types PIN-10UV and PIN-040a (United Detector Technology, Santa Monica, Calif.), and a PAR Model 134 Electrometer (Princeton Applied Research, Princeton, N.J.). Absolute calibrations of the light sources and of the photodiodes were performed with a Hewlett-Packard Model 8335A Radiant Fluxmeter (Hewlett-Packard Co., Palo Alto, Calif.).

Noise Generator and Noise Parameters

An electronic pseudorandom noise generator was constructed[1] to produce band-limited white gaussian noise. Its mixed digital-analog design permitted maximal freedom in selecting the noise parameters and in particular allowed operation at the very low frequencies corresponding to the response of *Phycomyces*.

In this series of papers, the same noise pattern was used for almost all experiments. The only exception was a series of experiments in this paper using three additional noise programs for comparison. For all four patterns the bandwidth (cutoff frequency) was 0.3 min^{-1}, a factor of two beyond the bandwidth of the growth response. Restriction of the noise bandwidth is necessary to reduce the statistical variance of the kernel estimates (Marmarelis and Naka, 1973). The repetition period of the noise patterns was 5.69 h, which exceeded slightly the analysis length of the experiments.

The voltage output of the noise generator was fed to the wedge servo to control the wedge angle. As a result the logarithm of intensity, $\log_{10}I$, was proportional to the white gaussian noise signal. The standard deviation of the gaussian amplitude distribution was σ = 0.57

[1] Lipson, E. D., K. W. Foster, and M. P. Walsh. 1975. A versatile pseudorandom noise generator. Submitted for publication.

decades ($\log_{10}$ units). To specify the reference intensity level for each experiment, define the "log-mean intensity" I_0 by

$$\log_{10} I_0 \equiv \langle \log_{10} I \rangle$$

where the brackets indicate a temporal average over the noise pattern.

Experimental Variables and Procedures

The raw data for each run consisted simply of the time series for the white noise stimulus and that of the velocity response. Both were available as voltages, the former from the wedge servo and the latter from the tracking machine servo. These voltages were digitized simultaneously at 10-s intervals and stored in the memory of a Fabri-Tek Model 1062 Instrument Computer (Nicolet Instruments, Madison, Wis.). Timing signals from the Instrument Computer were used to control the noise generator. Every 43 min the memory contents were dumped on magnetic tape. In addition, the stimulus and response were recorded on a strip chart recorder for examination during and after the run.

During the setup of each experiment (about 10 min) the wedge was held at its mean position so that the specimen would start adapting to the log-mean intensity. The experiment proper began when the Instrument Computer and noise generator were started. To permit the system to adapt further the first 45 min of the data records were ignored during analysis. During analysis the data records were truncated at 6.25 h. Therefore the portion analyzed was 5.5 h.

Data Analysis

The data were analyzed with the help of an IBM 2250 display terminal coupled to either an IBM 370/135 or more recently an IBM 370/158 computer. All programs were executed under control of a unique interactive software system at the Caltech Computer Center (McCann, 1973). Most of the programs used for the white noise analysis were the same as those in Marmarelis and Naka (1973).

Before the actual computation of the kernels the raw data records were preprocessed as follows. First several runs performed under identical conditions were averaged together. To reduce computation time the sampling (of the averaged data) was reduced to 20-s intervals. The runs were then truncated as mentioned above. Then both the stimulus and response were processed for removal of base-line trends by subtracting out a best fit quadratic function of time. For computational convenience the white noise stimulus amplitude was renormalized such that its power spectral density K was unity. The Wiener kernels were computed according to Eq. 2.

To evaluate how well the mathematical model provided by the empirical kernels was describing the system, the following tests were performed. The white noise stimulus and the kernels were applied to Eq. 1. The result was the prediction of the model for the same experiment. Mean square errors were computed between the *Phycomyces* response and the model response as a measure of the goodness of fit of the kernels. This procedure is analogous to evaluating a least-squares fit to a set of data points by examining the mean square deviation of the points from the fitted line.

Besides this time domain analysis, a complementary analysis was performed in the frequency domain. Power spectra were computed for the processed response data and the model response records. In addition the Fast Fourier Transform algorithm (Cooley and Tukey, 1965) was applied to the first order kernel to permit transfer function analysis.

In the course of analyzing the data it was discovered that specimens that happened to grow faster than average gave proportionately larger responses and, in turn, larger kernels. To

reduce systematic errors in comparing results, the response records and kernels in all three papers have been renormalized to a standard growth velocity of 45 μm/min. Specifically, the responses and kernels have been scaled by a factor $45/\overline{V}$ where $\overline{V}$ is the mean growth velocity for the given series of experiments. The values of $\overline{V}$ are available in tables in all three papers (here in Table I).

Analog Electronics

Electronic circuits were designed to simulate the system transfer function and adaptation dynamics. They were constructed using inexpensive integrated circuit components (Texas Instruments, Dallas, Tex.). The AD755P antilog amplifier was purchased from Analog Devices (Norwood, Mass.). To generate pulse, step, and sinusoidal test waveforms, a model 144 HF Sweep Generator (Wavetek, San Diego, Calif.) was used. A supplemental circuit was constructed to generate dark adaptation programs, which include a test pulse of variable delay, width, and amplitude.

The signals were conveniently observed together on an oscilloscope. The illustrations of circuit responses shown here were produced via the Fabri-Tek Instrument Computer and an *X-Y* recorder.

RESULTS

Time Domain Analysis

The standard white noise stimulus program is shown in Fig. 1 *a*. The experimental response, averaged for six runs and already processed for removal of base-line trends, is shown in Fig. 1 *b*. The records have been truncated at both ends as described earlier. One can readily see pronounced correlations between peaks and valleys in the stimulus and response records, with a time delay of a few minutes.

The Wiener kernels $h_1(\tau)$ and $h_2(\tau_1, \tau_2)$ computed from these data via Eq. 2 are

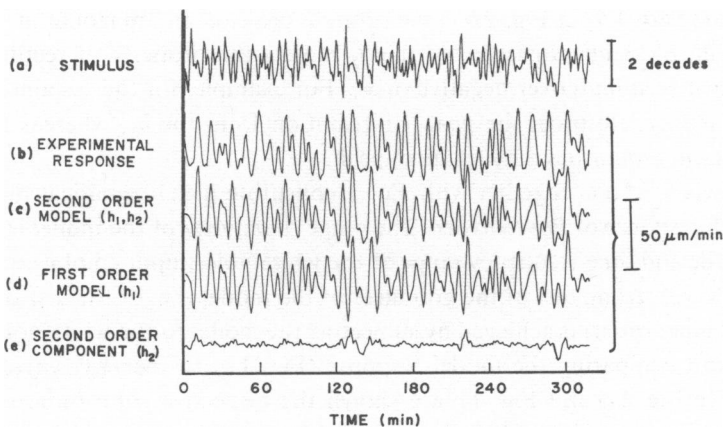

FIGURE 1 (*a*) The white noise stimulus program, which was applied to the input variable $\log_{10}(I(t)/I_0)$. (*b*) Response of *Phycomyces* to above stimulus, averaged over seven experiments. (*c*) Response of second-order Wiener model to above stimulus, using derived h_1 and h_2 shown in Fig. 2. (*d*) Response of first-order Wiener model. (*e*) Contribution of second-order kernel to model response. Curve *c* is the sum of curves *d* and *e*.

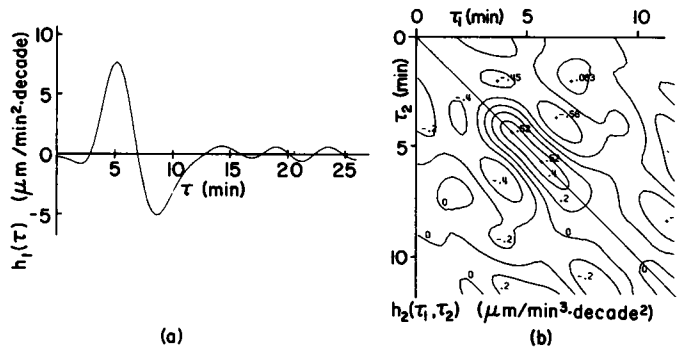

FIGURE 2 Wiener kernels of first order (*a*) and second order (*b*), derived by cross-correlations (Eq. 2) between the data in Fig. 1 curves *a* and *b*. The second-order kernel is represented as a contour plot. The units of the contour values are indicated below the plot. Because $h_2(\tau_1, \tau_2)$ is a symmetrical function the contours are labeled only in the bottom left half of the figure. The values in the upper right half are relative extrema. These conventions are followed for all second-order kernels illustrated in these papers.

displayed in Fig. 2. For any degree of nonlinearity, the first order kernel $h_1(\tau)$ is essentially the response to small pulse stimuli. As such it may be compared to the pulse response data of Foster and Lipson (1973). The asymmetrical biphasic response after a latent period of a few minutes is evident in Fig. 2*a*. For the kernel h_1 the latency appears to be about 3 min. The positive peak occurs at 5.3 min. The small undershoot during the latent period is attributable largely to the limited bandwidth of the white noise; that limitation was imposed to reduce the statistical variance of the kernels at the expense of this slight distortion. The net area of $h_1(\tau)$ is approximately zero. This feature is an expression of adaptation, as discussed below. The dominant feature of the kernel h_2 in Fig. 2*b* is the positive peak on the diagonal at $\tau_1 = \tau_2 =$ 5.8 min. This particular structure of the h_2 reflects the property of rectification, i.e. favoring positive stimuli over negative ones. For example, for the response to a positive pulse, the h_2 reinforces the peak contribution from the h_1, whereas for a negative pulse the h_2 diminishes the (negative) peak.

The kernels h_1 and h_2 together with Eq. 1 constitute a mathematical model of the light growth response of *Phycomyces*. The range of validity of the model is defined by the amplitude and time-frequency range of the white noise input employed in deriving it. A simple yet strong test of the goodness of the model (i.e. of the dispensability of kernels of higher order) is achieved by subjecting the model to the white noise stimulus (Fig. 1*a*) and comparing the model response (Fig. 1*c*) to the *Phycomyces* response (Fig. 1*b*). In Fig. 1*d* and Fig. 1*e* are shown the respective contributions of h_1 and h_2. The mean square errors (MSE) listed in Table I permit a numerical comparison of the Wiener models of each order.

The agreement between the *Phycomyces* and model responses is quite good. The first-order model is nearly as good as the second-order model. The smallness of the h_2 contribution and the quality of the first-order model indicate rapid convergence

TABLE I

COMPARISON OF RESULTS FOR FOUR WHITE NOISE STIMULUS PROGRAMS

Kernels in Fig.	White noise program	No. of exp.	Mean velocity	MSE of model response*			Time of h_1 peak	Peak amplitude	
				Zero order	First order	Second order		h_1	h_2
			$\mu m/min$	$(\mu m/min)^2$	%	%	min	$\frac{\mu m/min^2}{decade}$	$\frac{\mu m/min^3}{decade^2}$
2,3*a*	Standard	7	52	108	22.0	19.3	5.3	7.7	0.52
3*a*	No. 2	4	47	96	28.7	21.1	5.5	6.7	0.88
3*a*	No. 3	4	45	84	26.6	20.3	5.4	7.0	1.16
3*a*	No. 4	4	47	93	34.5	28.8	5.6	6.5	1.70
3*b*	Mean	—	48	—	—	—	5.4	7.0	1.02

*Mean square errors between experimental and model response records. MSE for zero-order model (h_0) is in absolute units. MSEs for first-order (h_1) and second-order (h_1, h_2) models are given as percentages of zero-order MSE.

of the Wiener series over the range tested. Thus in terms of log I the light growth response is reasonably linear.

In Fig. 1 the model slightly overpredicts the response amplitude for the first half of the experiment and underpredicts for the second half. This trend results from the gradual increase in the *Phycomyces* response during the course of the experiment, associated with the gradually increasing growth velocity. The effect of this trend on the kernel evaluation is not serious because of the *averaging* nature of the cross-correlation analysis. The Wiener functional series is unable to incorporate this slight nonstationarity. Thus the kernels may be thought of as representing the response characteristics at the mean time of the experiment, or alternatively the average throughout the experiment.

With the exception of the following, all experiments in this series of papers were performed with the standard white noise stimulus program shown in Fig. 1*a*. Thus kernels obtained under different experimental conditions can be compared to those of Fig. 2 without errors due to variations between the noise programs. However, to determine the degree to which the kernels depend on the choice of noise program three additional programs were employed under otherwise identical conditions. For each program four identical experiments were performed and averaged prior to kernel computation. The first-order kernels for the four independent programs are shown in Fig. 3*a*. The average of the four kernels is shown in Fig. 3*b* along with the average of the corresponding second-order kernels in Fig. 3*c*. Because of the averaging nature of the Lee-Schetzen correlation analysis, these averaged kernels are statistically equivalent to kernels from a single experiment with the four stimulus programs concatenated. Moreover the average kernels provide a more accurate representation of the light growth response functional. Comparing the standard and average kernels $h_1(\tau)$ one sees slight differences in both amplitude and shape. In particular the oscillations occurring late in the standard kernel appear less significant in the more accurate aver-

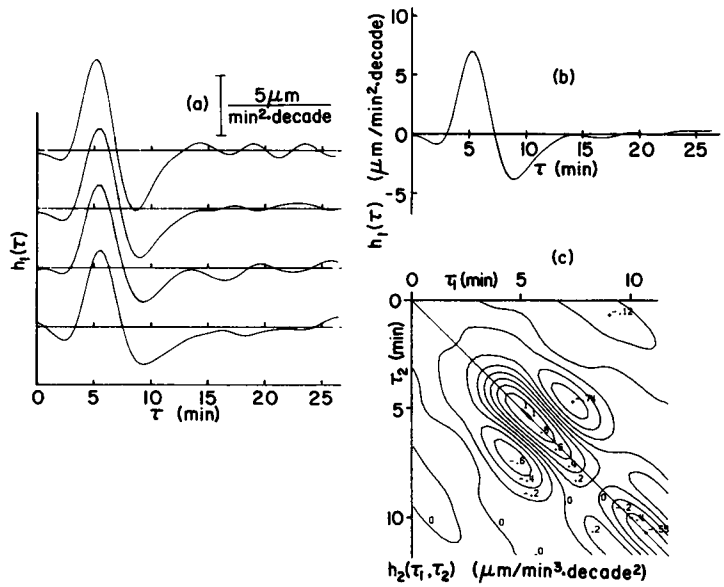

FIGURE 3 (*a*) Comparison of first-order kernels for four independent, but stochastically equivalent, white-noise stimulus programs. The upper-most kernel is the standard kernel of Fig. 2 *a*. The average of the four kernels is shown in *b*. For brevity the individual second-order kernels are not shown. Their average, shown in *c*, may be compared with the standard kernel in Fig. 2 *b*.

age kernel. In the system analysis which follows, the average kernel h_1 will be used because of its high accuracy. Results for the standard kernel will be needed for comparison with results in papers II and III. However the results obtained from the average kernel, which is available only for the present experimental conditions, are preferred over those for the standard kernel.

Frequency Domain Analysis

In studying systems it is profitable to examine features in both the time and frequency domains with the aid of Fourier or Laplace transforms. In particular, systems are usually simpler to recognize and combine with one another in the frequency domain. Since the first order kernel $h_1(\tau)$ alone offers a reasonably accurate description of the light growth response system, the analysis here will be presented mainly within the framework of linear system theory. The response characteristics in the frequency domain will be presented in two closely related forms: (*a*) the power spectrum of the response to a white noise stimulus and (*b*) the linear model "transfer function."

For a *linear* system with input $x(t)$ and output $y(t)$, the transfer function $H_L(f)$ is defined (Goldman, 1953) as the ratio of the respective complex Fourier transforms $X(f)$ and $Y(f)$:

$$H_L(f) = Y(f)/X(f)$$

assuming initial conditions of zero. The Fourier transform of $H_L(f)$, denoted by

$h_L(t)$, is the "impulse response" of the linear system (Goldman, 1953). White noise analysis of any linear system would give a first order Wiener kernel $h_1(t) \equiv h_L(t)$ and all higher order kernels would vanish.

If $P_X(f)$ and $P_{Y,L}(f)$ are the respective power spectra for $x(t)$ and $y(t)$ then it can be shown (Blackman and Tukey, 1958) that

$$P_{Y,L}(f) = |H_L(f)|^2 P_X(f). \tag{3}$$

Now, if $x(t)$ is a white noise signal then $P_X(f) = K$, a constant. Therefore

$$P_{Y,L}(f) = K\,|H_L(f)|^2,$$

or

$$20 \log_{10} |H_L(f)| = 10 \log_{10} P_{Y,L}(f) - 10 \log_{10} K, \tag{4}$$

where each term is written explicitly in "units" of decibels (dB). Thus, within the approximation that the system is linear with log I, the power spectrum of the linear model response to white noise may be viewed also as a Bode plot (Milsum, 1966) of the transfer function $H_L(f)$. It is simpler and more common to express transfer functions in terms of the Laplace transform variable $s = j2\pi f$, where $j = (-1)^{1/2}$.

In Fig. 4 are shown double-logarithmic plots of the power spectra for the top four curves of Fig. 1, namely the stimulus, *Phycomyces* response, second-order model re-

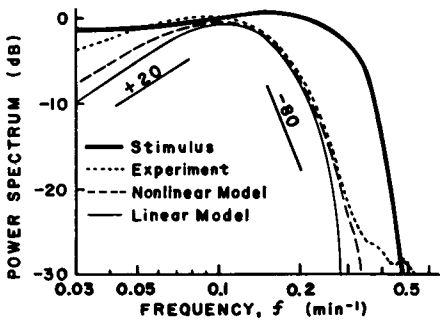

FIGURE 4

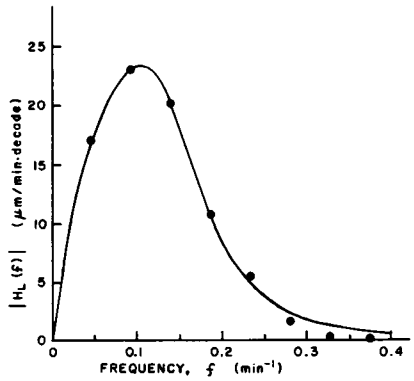

FIGURE 5

FIGURE 4 Power spectral densities for stimulus and response records of Fig. 1 (*a–d*). The units corresponding to 0 dB are, respectively, 1 decade^2/min for the stimulus power spectrum and 730 μm^2/min for the response power spectra. Slopes of +20 dB/decade and −80 dB/decade are indicated as aids in the transfer function analysis (see text).

FIGURE 5 Frequency domain analysis of first-order kernel, treated as a linear model transfer function. The amplitude of the Fourier transform of the averaged kernel of Figure 3 *b* is shown by the dots. The values have been fit to the amplitude (Eq. 7) of the fifth-order system represented by Eq. 6. The curve is the result of the fit, i.e. a plot of Eq. 7 with the deduced parameters as given in the text.

sponse, and first-order model response. Note that only the latter two depend on the kernel computation. The deviations at low and high frequencies of the *Phycomyces* power spectrum from the model response spectra may be attributed to random fluctuations, drift, and to a lesser extent to truncation of the kernels and to neglect of higher order kernels. For the present experiments at $I_0 = 10^{-6}$ W/cm^2, the response has a cutoff frequency (defined by 3 dB attenuation relative to the peak) of 0.15 min^{-1}. Focusing on the model response power spectra of first and second order, one observes at low frequency a gradual rise of about 20 dB/decade and beyond the cutoff frequency a precipitous rolloff of 80 dB/decade or greater. These log-log slopes suggest a linear model transfer function of the general form:

$$H_L(f) = H_L\left(\frac{s}{2\pi j}\right) = \frac{s\phi(s)}{a_0 + a_1 s + a_2 s^2 + a_3 s^3 + a_4 s^4 + a_5 s^5}, \tag{5}$$

where $\phi(s)$ is a "nonminimum phase" term with magnitude unity and the a_i are constants. Thus the system is roughly *fifth order*, i.e. described by a fifth-order linear differential equation. As will be shown in the next section and the Appendix, the long-term dark adaptation experiments of Delbrück and Reichardt (1956) suggest a similar adaptive element of the form $s/(s + 1/b)$, corresponding to a first-order high-pass filter with a time constant b. Assuming such an element occurs first, the rest of the pathway could then be expressed as a fourth-order low-pass filter following the adaptive (high-pass) element. A preliminary Bode analysis (Milsum, 1966) of Fig. 4 suggested the following form:

$$H_L(f) = \beta e^{-st_0}\left[\frac{s}{s + 2\pi f_1}\right]\left[\frac{(2\pi f_2)^2}{s^2 + 2\alpha(2\pi f_2)s + (2\pi f_2)^2}\right]^2 \tag{6}$$

with $s = 2\pi j f$; i.e. a first-order high-pass filter with cutoff frequency f_1 followed by two identical second-order low-pass filters with undamped natural frequency f_2 and damping ratio α. The adaptation time constant b is related to the adaptation cutoff frequency f_1 by $b = 1/2\pi f_1$. The constant β, which sets the gain of the system, is in the same units as $H_L(f)$. The phase term e^{-st_0} is included to allow for the latency of the light growth response and will be evaluated separately below.

For the estimation of the parameters f_1, f_2, α and β, the average kernel $h_1(t)$ of Fig. 3 *b* was used. The Fast Fourier Transform algorithm (Cooley and Tukey, 1965) was applied to the first 64 points (21.3 min) of $h_1(t)$ to obtain the Fourier transform $H_1(f)$. Then the amplitude $|H_1(f)|$, shown by black dots in Fig. 5, was fit by a nonlinear least squares procedure (Hamilton, 1964) to the following form for the amplitude of $H_L(f)$:

$$|H_L(f)| = \frac{\beta f_2^4 f}{(f^2 + f_1^2)^{1/2}[(f^2 - f_2^2)^2 + (2\alpha f_2 f)^2]}. \tag{7}$$

The resulting parameter values are

$$\beta = (20 \pm 3)\,\mu\text{m/min} \cdot \text{decade},$$
$$f_1 = (0.037 \pm 0.013)\,\text{min}^{-1},$$
$$f_2 = (0.156 \pm 0.004)\,\text{min}^{-1},$$
$$\alpha = 0.54 \pm 0.04.$$

In Fig. 5 the curve of Eq. 7 with these parameter estimates agrees well with the data points for $|H_1(f)|$. The value of f_1 corresponds to an adaptation time constant b = (4.2 ± 1.5) min. The undamped natural frequency f_2 is very close to the system cut-off frequency of 0.15 min^{-1}. The result that α is less than unity implies that the second-order systems are underdamped. The resonant frequency of each second-order system is $f_2(1 - 2\alpha^2)^{1/2}$ = (0.10 ± 0.01) min^{-1}, close to the peak of the system transfer function. The decay time constant of each system is $1/(2\pi f_2 \alpha)$ = (1.9 ± 0.2) min, somewhat shorter than the adaptation time constant.

The electronic circuit shown schematically in Fig. 6 *a* was constructed to simulate the linear transfer function of Eq. 6. The time delay t_0 appearing in the phase term e^{-st_0} has been evaluated with the help of the circuit. The impulse response of the circuit, shown in Fig. 6 *b*, aligns well with the kernel h_1 for a latency value of t_0 = 2.5 min. The agreement supports the assumption implicit in Eq. 6 that the nonminimum phase of the system can be expressed simply as $\phi(s) = e^{-st_0}$. For comparison, t_0 was determined directly from the frequency domain data; ϕ was taken as the difference be-

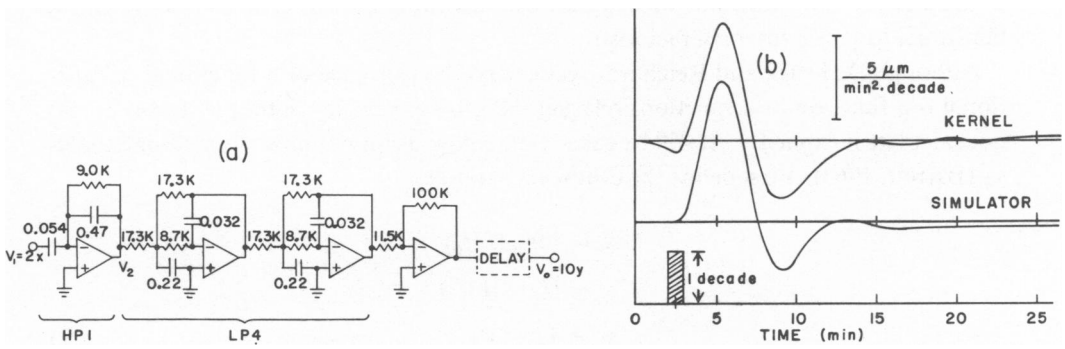

FIGURE 6 Linear electronic simulation of light growth response. (*a*) Electronic representation of linear-model transfer function of Eq. 6. The dynamics of the system are contained in the first-order high-pass filter (HP1) and the fourth-order low-pass filter (LP4). The latter is composed of two identical second-order low-pass filters in cascade. The inverting amplifier restores the polarity and sets the overall gain of the system to correspond to the value of the gain parameter β. For convenience the time units have been scaled 1 ms:1 min. The conversion factors for the voltages are 1 V:2 decades for V_1, and 1 V:10 μm/min for V_0. The delay is achieved artificially by redefining the time origin of the output. (*b*) Response of the circuit (lower curve) to a unit pulse (1 decade for 1 min) compared to the average kernel from Fig. 3 *b*. The curves correspond best temporally with a delay of 2.5 min, applied to the circuit response, as shown. The time and amplitude units of the circuit response have been converted to match the kernel units.

tween the phase of $H_1(f)$ (data not shown) and the minimum phase corresponding to the amplitude $|H_L(f)|$ in Eq. 7. A straight-line fit of $\phi(s)$ vs. frequency gave a slope $t_0 = (2.6 \pm 0.1)$ min in good agreement with the above value.

In Fig. 4 the characteristics of the nonlinear model response power spectrum do not differ greatly from those for the linear model. In particular the rising slope is also 20 dB/decade and the roll-off is also about 80 dB/decade. Thus one would expect the general features elaborated above to apply to the nonlinear system with the allowance that some of the reactions must be somewhat nonlinear.

Adaptation

The light response system of *Phycomyces* exhibits adaptation over about nine decades of light intensity, comparable to the adaptation range of vertebrate vision. Delbrück and Reichardt (1956) conducted dark adaptation experiments which they interpreted with the following model. They defined an internal state variable A, the "level of adaptation," as either the constant intensity to which the system had been adapted or more generally the virtual intensity to which the system seemed (by responses to test pulses) to have been adapted at a given time. The growth response then depended functionally only on the "subjective intensity" I/A (or equivalently $(I - A)/A$, which is preferred here). Their experiments suggested that the dynamics of adaptation are contained in the differential equation

$$dA/dt = (I - A)/b \tag{8}$$

where b is the time constant of adaptation. According to Eq. 8, A follows I with a first-order low-pass filter characteristic.

Although Delbrück and Reichardt recognized the existence of a functional (a functional is a function of a function) relating the growth velocity output to I/A they did not calculate it explicitly. It will be calculated below using nonlinear functional analysis (Barrett, 1963). First define the following variables

$$\begin{aligned} x &= \log_{10}(I/I_0), \\ z &= (I - A)/A, \\ y &= V - V_0 \end{aligned} \tag{9}$$

where I_0 is a reference intensity, $V(t)$ is the growth velocity and V_0 is its steady-state level. In terms of these variables the model is expressed in Fig. 7*a*. The light growth response system, indicated by the functional **H** is decomposed conceptually into two subsystems **F** and **G** operating in cascade. The "adaptation functional" **F** operates on the input x to produce z. The "output functional" **G** in turn operates on z to produce y.

In the Appendix expressions are derived for the kernels of first and second order of the adaptation functional **F**. The first-order kernel f_1 acts as a first-order high-pass

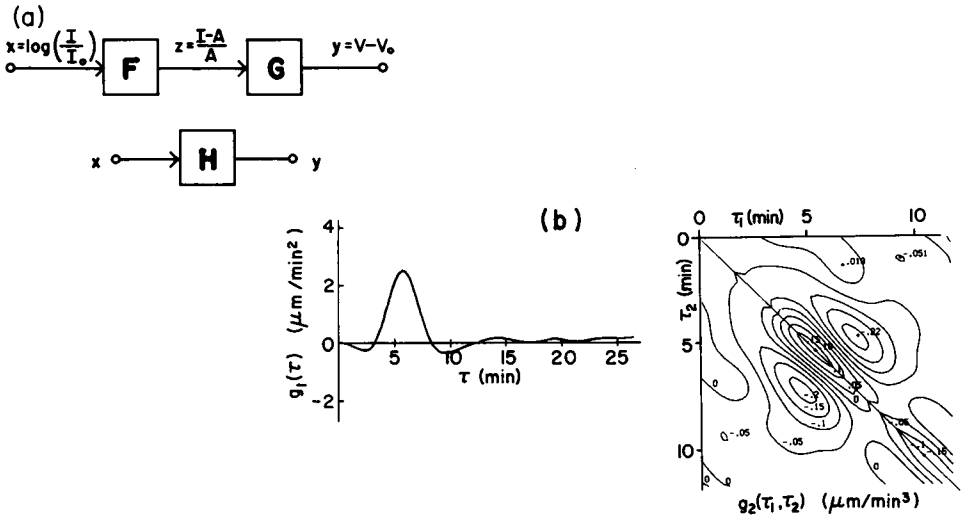

FIGURE 7 (*a*) Decomposition of functional **H** for the light growth response pathway into functionals **F** and **G** in cascade. The adaptation model is represented by **F**. The internal variable z is the subjective intensity. (*b*) Kernels $g_1(\tau)$ and $g_2(\tau_1, \tau_2)$ for **G**, derived from those for **F** and **H**.

filter with time constant b. The second-order kernel f_2 behaves as a nonlinear high-pass filter. The transform of $f_1(t)$, namely $F_1(s) = abs/(1 + bs)$, was anticipated in the transfer function analysis in the previous section. Using the first-order kernel of Fig. 3*b*, the transfer function fit produced the value $b = (4.2 \pm 1.5)$ min, consistent with the value $b = 3.8$ min reported by Delbrück and Reichardt (1956) for dark adaptation experiments.

It is shown in the Appendix how the output functional **G** may be unfolded from the empirical **H** and theoretical **F**. The kernels $g_1(\tau)$ and $g_2(\tau_1, \tau_2)$ derived using Eq. 17 are shown in Fig. 7*b*,*c* assuming $b = 4.2$ min. In the linear approximation, the kernel $g_1(\tau)$ is essentially the impulse response of the fourth-order low-pass filter described in the previous section. Since f_1 and f_2 are practically monotonic functions the fine structures of h_1 and h_2 are carried over in part to g_1 and g_2. However one notices in g_1 the absence of further high-pass filtering. This is consistent with the 20 dB/decade initial rise of the response power spectrum (Fig. 3), which indicates but a single order of high-pass filtering. The consequence of this feature is that if the input to **G**, namely $z = (I - A)/A$, is held constant, then the growth velocity should remain elevated. The input condition that would make z constant (in the steady-state) is that $x(t)$ be a ramp function, or that $I(t)$ be an exponential function, as in the so-called "sunrise experiments" (Bergman et al., 1969). Indeed it is found in these sunrise experiments that the growth velocity *does* remain elevated.

It should be pointed out that dark adaptation programs are very different in character from the white noise stimulus programs used to obtain the kernels. As will be discussed in the following paper, the dynamic range of the gaussian white noise stimuli is

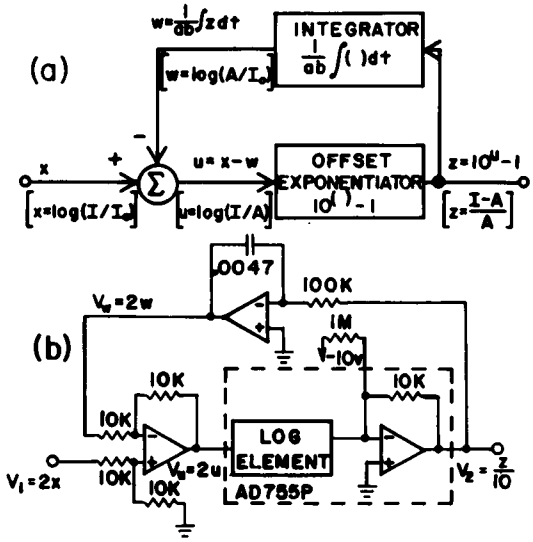

FIGURE 8 (*a*) Representation of adaptation functional as a feedback system, based on Eq. 10. The relations in parentheses are obtained using Eq. 8 and Eq. 9. The design is implemented in an electronic circuit (*b*), which serves as a nonlinear generalization of the high-pass filter in Fig. 6 *a*. As before, the time scale has been compressed 1 ms:1 min. The conversion factors for the voltages (in volts) are shown on the figure. Note that x, u, w, and z are dimensionless variables. The components within the dashed rectangle constitute an Analog Devices 755P log/antilog amplifier. The other amplifiers are SN72741 operational amplifiers. The relation between V_2 and V_3 is $V_2 = -0.1\,(10^{V_3/2} - 1)$.

comparatively small. Within the range of a few decades, adaptation has been associated here with a high-pass filter with a time constant of roughly 4 min. As part of its role in the system dynamics this adaptation filter accounts for the phenomenon that the steady-state response to a step change in intensity is zero; in other words, the steady-state growth velocity is independent of intensity (except at very high intensity; Foster and Lipson, 1973).

The adaptation functional F can be represented exactly by the simple feedback circuit shown in Fig. 8 *b*. The design of the circuit was based on the observation that the differential equation 11 has a simple inverse solution for x in terms of z, namely

$$x = \frac{1}{ab}\int_0^t z\,dt + \log_{10}(1 + z). \tag{10}$$

Using the relations in the explanatory block diagram of Fig. 8 *a*, it is easy to show that the circuit satisfies this equation. Note that the nonlinearity and the "memory" are isolated respectively in the offset exponentiator and in the integrator. As a bonus the circuit provides two important signals within the feedback loop: $w(t)$ and $u(t)$ are logarithmic measures respectively of the "level of adaptation" A and the "subjective intensity" I/A (Delbrück and Reichardt, 1956).

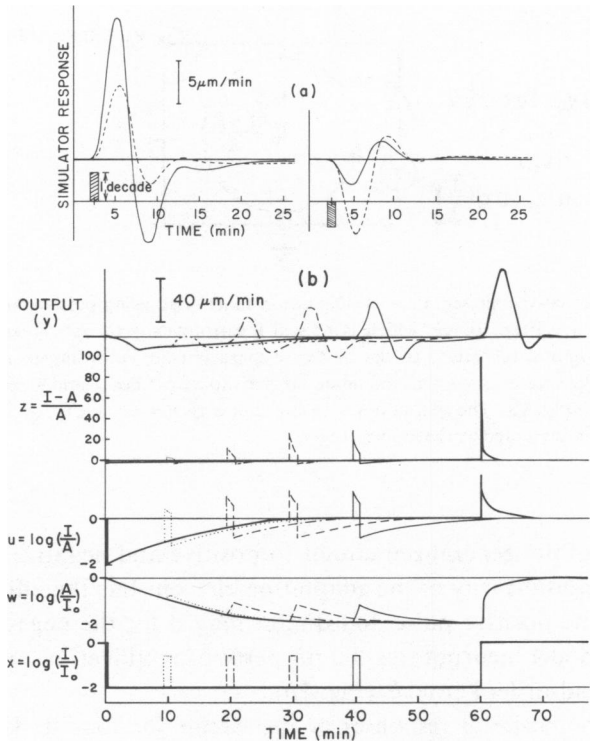

FIGURE 9 (*a*) Pulse responses (solid curves) of generalized analog circuit, with adaptation element of Fig. 8*a* substituted for high-pass filter in Fig. 6*a*. The magnitude of the unit pulses corresponds to 1 OD for 1 min, of either polarity. The dashed curves show the responses of the original linear circuit of Fig. 6*a* for comparison. The nonlinearity of the adaptation element manifests itself as rectification. (*b*) Response of generalized simulator circuit to four dark adaptation programs (lower curve) shown in composite. In the description of the circuit here, the units from the circuit have been converted to those appropriate for *Phycomyces*. At $t = 0$, the "intensity" was dropped 2 OD and at $t = 60$ min it was restored to the initial level. Test pulses of width 1 min and amplitude 1.5 OD were given alternatively at $t = 10$, 20, 30, or 40 min. For brevity the pulses and their effects are superposed on the one figure. The three middle curves show signals from the adaptation network: respectively, A/I_0 and I/A, both logarithmically, and $(I - A)/A$. The result of applying the last signal to the fourth-order low-pass filter in Fig. 6*a* is shown by the upper curve (output).

In the linear circuit of Fig. 6*a*, the high-pass filter at the input represented the first-order approximation of the adaptation functional **F**. Indeed for small signals the adaptation circuit just presented becomes functionally equivalent to that filter. Thus the simulator circuit of Fig. 6*a* may be generalized to large-scale signals by substituting the nonlinear adaptation element for the linear high-pass filter. Residual nonlinearities, in the remainder of the circuit of Fig. 6 (functional **G** of Fig. 7), are not incorporated into the refined circuit. However the circuit, with only the nonlinearity of the adaptation model, does quite well at simulating the large-scale nonlinear behavior of *Phycomyces*.

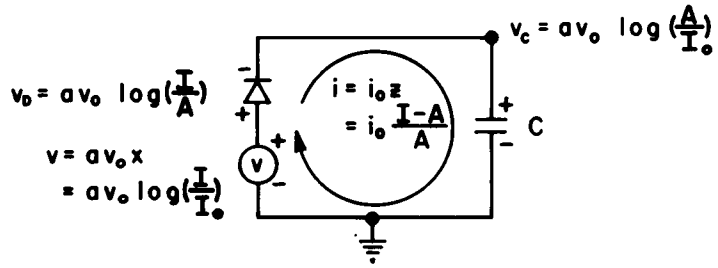

FIGURE 10 Alternative representation of adaptation functional, using passive components. The circuit contains a voltage source, which is related logarithmically to light intensity as shown. The parameters i_0 and v_0 pertain to the diode i-v characteristic, according to $i = i_0 (\exp(v_D/v_0) - 1)$. The relationships shown on the figure are derivable from Eqs. 8 and 9 and are analogous to those shown in Fig. 8 *a*. The adaptation time constant is given by $b = Cv_0/i_0$. The output z of the functional is represented by the loop current i.

The response of the generalized circuit to positive and negative pulses is shown in Fig. 9 *a*. The nonlinearity of the adaptation element has the effect of enhancing the response to the positive pulse and diminishing it for the negative pulse. Thus the adaptation model incorporates the property of rectification, which was recognized in the second-order kernel h_2 (Fig. 2 *b*).

Fig. 9 *b* is a composite of responses of the circuit for four dark adaptation test programs (Delbrück and Reichardt, 1956). Each repetition of the program consists of a step down, a test pulse, and a step up. The solid curves represent the behavior in the absence of a test pulse. The negative step at $t = 0$ is seen to produce a shallow but prolonged response (upper curve) compared with the positive step at $t = 60$ min. The source of the difference can be found in the intermediate curves, which show very different time courses for the steps down and up. Comparing the effects of the test pulses, one sees the system is effectively readapted by $t = 30$ or 40 min, since the responses for those times are practically the same. The reduction of the responses for $t = 10$ min and 20 min can be traced to the intermediate curves, in particular the adaptation output $(I - A)/A$. The simulator will be helpful in planning and interpreting experiments to test the adaptation model with these and other adaptation programs at various intensity ranges as well as sunrise programs, mentioned earlier.

In the adaptation system described in Fig. 8, the offset exponentiator has an input-output relation similar to the current-voltage (i-v) characteristic of a solid-state rectifier, namely $i = i_0 (\exp(v/v_0) - 1)$ where i_0 is the reverse bias current and $v_0 = kT/e = 25$ mV. For consistency the feedback integrator would then have a current input and voltage output and be representable simply by a capacitor. Indeed the adaptation functional may be represented alternatively by the simple passive circuit of Fig. 10. While the circuit of Fig. 8 *a* is preferred for precise simulation of adaptation, the present circuit is of interest because it suggests a possible biological context for *Phycomyces* adaptation, as will be discussed below.

DISCUSSION

It was Wiener (1958) who first recognized white gaussian noise as the optimum test signal for the identification of nonlinear systems. Stimulation with white noise best approaches the ideal of testing a system uniformly with all possible variations of the input. The measurement time is exploited much more efficiently with white noise than with occasional pulses or repetitive sinusoidal stimuli. The white noise analysis method strongly rejects random fluctuations appearing in the response record.

In papers II and III results will be compared for a number of experimental conditions and strains. For this purpose, the kernels provide a compact, objective, and accurate representation of the characteristics in each circumstance. Compared with conventional stimuli, white gaussian noise offers an important additional advantage. In pulse experiments, for example, one is tempted to use a large standard stimulus to produce significant responses. As a result one tends to drive the system into saturation and lose the small-scale aspects of the response which are usually simpler (i.e. linear) and more representative of the natural behavior of the system. The gaussianness of the white noise on the other hand gives emphasis to the small-scale behavior. Thus while the method is equipped to characterize nonlinearities, it is also well suited to extracting the small-signal characteristics of the system.

On the other hand the white noise method is subject to several practical limitations. The white noise stimulus must always be restricted in its bandwidth, duration, and amplitude range. These constraints limit the accuracy and generality of the results. Moreover restrictions on computation time and computer memory limit the order to which kernels may be calculated. In the present work, the analysis was carried to second order. Even when computation of higher order kernels becomes necessary, kernels of higher than second order are awkward to display. A frequency domain method for computing Wiener kernels has been proposed by French and Butz (1973). The increased computation efficiency of this method relative to time-domain correlation analysis may permit a few more kernels to be computed when necessary. Truncation of the Wiener series at low order limits application of the white noise method to systems that are nearly linear within the range studied. This condition was fulfilled in the present study.

The first order kernel $h_1(\tau)$ accounts for most of the response to the white noise stimulus. Since the input variable was log I, one concludes that the system is approximately linear with log I over the tested range of a few decades. This lends support to the conjecture that there is a logarithmic transducer early in the light response pathway (Foster and Lipson, 1973; Bergman et al., 1973). Such logarithmic range compression is a common feature of sensory systems and is often expressed in terms of the Weber-Fechner relation.

The shape of $h_1(\tau)$ in Fig. 2*a*, as expected, resembles that of responses to pulse stimuli, particularly smaller stimuli which do not saturate the response (Foster and Lipson, 1973). In particular one observes the pronounced biphasic response after a latent period of about 2.5 min. The approximate equality of the areas of the positive

and negative phases of $h_1(\tau)$ ties in closely with the phenomenon of adaptation. The structure of the second-order Wiener kernel $h_2(\tau_1, \tau_2)$ in Fig. 2*b* is dominated by a diagonal peak which corresponds temporally to the peak of $h_1(\tau)$. As such the h_2 reveals the static nonlinearity of rectification, i.e. the property that positive stimuli elicit larger responses than do negative stimuli.

Further insight into the system dynamics was gained by examination of characteristics in the frequency domain. The approximate linearity of the system (with respect to the input variable log I) permitted the application of linear system theory. The power spectra of the experimental and model responses to white noise revealed that the slow dynamics of the system are of about fifth order. In other words the system is describable approximately by a fifth-order linear differential equation. In the frequency domain the input-output relation, defined by the linear differential equation, may be represented as a transfer function. The transfer function amplitude is closely related to the power spectrum of the response to white noise. Alternatively the transfer function can be obtained as the Fourier transform of $h_1(\tau)$. The first-order rise of the power spectrum at low frequency indicated the feature of adaptation, or high-pass filtering. The sharp roll-off above the cutoff frequency of 0.15 min^{-1} established the high order of the system.

A representative analytical form (Eq. 6) was taken for the system transfer function and fit to the Fourier transform of $h_1(\tau)$. The parameters evaluated from the fit include an adaptation time constant of about 4 min for the first-order high-pass filter, in agreement with the value of 3.8 min deduced from dark adaptation experiments (Delbrück and Reichardt, 1956). The remainder of the transfer function was described by an underdamped fourth-order low-pass filter. This linear model transfer function was implemented into an analog circuit (Fig. 6*a*) which simulates well the small-signal response characteristics. The high-pass filter at the input represents the linear aspect of adaptation corresponding to the kernel $f_1(\tau)$ of the adaptation functional **F**. The fourth-order low-pass filter corresponds to the kernel $g_1(\tau)$ of the output functional **G**. The high-pass filter was generalized to a nonlinear feedback network which incorporated the nonlinear adaptation model exactly. The functional of this adaptation model could also be represented by a simple circuit including a passive rectifier and capacitor (Fig. 10). The circuit elements suggest the possibility that adaptation might be governed by the currents and potentials of a biological membrane containing the photoreceptor. Biomembranes are well known for their high capacitance of about 1 $\mu f/cm^2$. Moreover rectification is a major nonlinearity of biomembranes (Cole, 1968) and of suitable model membranes (Müller and Rudin, 1968). However, in the case of membrane rectification, the *i-v* characteristics tend to be steeper than those for solid-state rectifiers. Instead of v_0 = 25 mV one finds typically v_0 = 4 mV (Eisenberg et al., 1973), presumably because of cooperativity of about six charges in the molecules which constitute membrane channels.

Imagine then that the circuit of Fig. 10 represents the electrical properties of a patch of some membrane in *Phycomyces* that houses the photoreceptor. The capacitance of the patch as a whole would be C and the membrane potential would be v_c, which is

proportional to the logarithm of the level of adaptation. Note, incidentally, that if $v_0 \approx 4$ mV, then v_c would change by $av_0 \approx 10$ mV for each decade of A. Thus for the range of about 10 decades over which *Phycomyces* adapts, v_c would span about 100 mV, comfortably within the voltage range of biomembranes.

In parallel with the capacitance is a series combination of a rectifier and a light-dependent voltage source. In terms of the hypothetical membrane, this combination could represent the net effect of a set of specialized ion channels. For example, one could imagine that (*a*) the photoreceptor molecules are membrane-bound proteins that comprise gateable ion channels, (*b*) the passive electrical properties of the channel can be represented by a rectifier, and (*c*) the photoreceptors can generate a potential which depends logarithmically on the light intensity. (The last property is just how solid-state photodiodes behave in their photovoltaic mode.)

The model, which is purely speculative, is presented with the hope that serious attempts will be undertaken to measure light-dependent membrane potentials in *Phycomyces* with this tentative concept in mind. Such a finding would have important implications for the role of *Phycomyces* as a model system for sensory processes.

For unsymmetric stimuli the light growth response is believed to be responsible also for phototropism. Other phenomena which play a part in phototropism include (*a*) focusing of light by the cylindrical optics of the sporangiophore, (*b*) local adaptation around the photosensitive growing zone, and (*c*) spiral growth, which causes the photoreceptors to rotate through a nonuniform light field and to induce local growth responses (Dennison and Bozof, 1973).[2]

The large adaptation range of the light growth response permits the sporangiophore to adjust its sensitivity to the ambient light level from twilight to bright sunlight. In the presence of unilateral light, the variations in intensity induced internally span a relatively narrow range. Therefore, the linear model transfer function and simulator circuit are presumably valid for describing the relative range for which the light growth response dynamics have been "designed." The first-order kernel and the derived models should be useful for deeper study of the relationship between the light growth response and phototropism. Furthermore the nonlinear circuit which represents the exact adaptation model serves as a guide for the planning and interpretation of specialized experiments to investigate the large scale adaptation capability of the light response system.

At this point it is worth reviewing the proposed elements of the system and speculating on their order in the stimulus-response pathway. Both the logarithmic transducer and the nonlinear adaptation element are presumed to lie early in the pathway. In paper II a model will be presented that ties adaptation to the photochemical kinetics of the photoreceptor; that is the earliest possible step where adaptation might occur. Conceivably the logarithmic transducer may be an integral part of the adaptation element since both are concerned with range compression. There must be at least one

[2] Dennison, D. S., and K. W. Foster. 1975. Intracellular rotation and the phototropic response of *Phycomyces*. In preparation.

linear step prior to the logarithmic transducer, for the very absorption of light by the photoreceptor molecules is a linear process, i.e., quantum counting by the pool of pigment molecules. The primary transduction step whereby the energy of the excited chromophore is converted into biochemical energy is likely to be where the processes of logarithmic transduction and adaptation reside. These processes may well involve either membranes or enzyme control or both. There is good reason to believe that the delay element and low-pass filter occur near the output of the pathway. The avoidance response, which has been shown by mutants to feed into a common growth control pathway (Bergman et al., 1973) shows a similar latency and time course (Cohen et al., 1975). In addition the stretch response (Bergman et al., 1969) shows a similar latency.

The high dynamic order of the system implies a moderate number of rate-limiting reactions with time constants of a few minutes, tailored through evolution to produce suitable local growth responses. Ultimately the dynamics studied here should be explicable in terms of molecular processes including, for example, membrane gating and enzyme control.

The slowness of the growth response of *Phycomyces* permits the time course of associated biochemical variables to be studied in real time, following an exposure to light. For example, Cohen (1974) has observed a transient decrease in cAMP concentration within the first 2 min following a step-up of light intensity. As another example, Jan, Forgac, and Lipson (unpublished observations) found a sustained increase in chitin synthetase activity by about 20% at high intensity (20 mW/cm^2 at λ = 488 nm), at which the growth velocity of sporangiophores remains elevated by a comparable amount (Foster and Lipson, 1973). That finding supports the hypothesis that control of chitin synthesis is the output of the light response pathway.

Toward the ultimate goal of defining the biochemical steps of the stimulus-response pathway, it is important to relate such biochemical effects to the dynamics of the light response. Thus for Cohen's results, the transient nature of the effect after a *step* increase in light suggests that cAMP is associated with the pathway at a later point than the adaptation step. The time span of the effect is shorter and earlier than a growth response. Thus the putative cAMP step cannot occur very late in the pathway. In the linear circuit analog (Fig. 6*a*), this step would correspond best with the output of the high-pass filter, thus preceding the low-pass filters and delay element. Indeed the time course of the cAMP effect is remarkably similar to the response $(I - A)/A$ of the nonlinear adaptation circuit to a step-up in intensity (Fig. 9*b*). It is hoped that additional biochemical correlates will be discovered and analyzed to elucidate the molecular processes responsible for the light response characteristics.

APPENDIX

Functionals for Delbrück-Reichardt Adaptation Model

In Fig. 7 the light growth response system H was decomposed hypothetically into two subsystems **F** and **G** in cascade. The system functionals considered as mathematical operators (Barrett, 1963) are related by

$$\mathbf{H} = \mathbf{G} * \mathbf{F},$$

where the asterisk denotes operator multiplication. If we denote the inverse of **F** by $\mathbf{K} \equiv \mathbf{F}^{-1}$ then **G** may be unfolded formally as

$$\mathbf{G} = \mathbf{H} * \mathbf{K}.$$

In this appendix we will derive expressions for the first and second order Wiener kernels for the functionals **F**, **K**, and **G**.

Using Eq. 9, Eq. 8 may be converted to the equivalent nonlinear differential equation

$$b\dot{z} + z^2 + z - abz\dot{x} - ab\dot{x} = 0, \tag{11}$$

where the dots denote time derivatives and $a = \ln 10 = 2.303$. Note that the definitions of x, z, and y ensure that all constant terms vanish for the associated Wiener series.

For the evaluation of and operations with the kernels it is advantageous to work in the frequency domain using Laplace transforms (Barrett, 1963; Brilliant, 1958). The solution of the above differential equation for the transformed kernels of **F** is

$$\begin{aligned} F_1(s) &= abs/(1 + bs), \\ F_2(s_1, s_2) &= \frac{a^2b^3s_1s_2(s_1 + s_2)}{2(1 + bs_1)(1 + bs_2)(1 + bs_1 + bs_2)}. \end{aligned} \tag{12}$$

The corresponding time-domain kernels are

$$\begin{aligned} f_1(t) &= a(\delta(t) - [1/b]e^{-t/b}), \\ f_2(t_1, t_2) &= a^2([1/b^2]e^{-(t_1+t_2)/b} + 1/2[\delta(t_1)\delta(t_2) - [1/b]e^{-t_2/b}\delta(t_2 - t_1) \\ &\quad - [1/b]e^{-t_1/b}\delta(t_2) - [1/b]e^{-t_2/b}\delta(t_1)]) \end{aligned} \tag{13}$$

where $\delta(t)$ is the Dirac delta function.

The relation of the kernels of **F** to those of its inverse **K** are (Brilliant, 1958)

$$\begin{aligned} K_1(s) &= 1/F_1(s), \\ K_2(s_1, s_2) &= -F_2(s_1, s_2)/F_1(s_1)F_1(s_2)F_1(s_1 + s_2). \end{aligned}$$

Therefore

$$\begin{aligned} K_1(s) &= (1 + 1/bs)/a, \\ K_2(s_1, s_2) &= -1/2a, \end{aligned} \tag{14}$$

and in the time domain

$$\begin{aligned} k_1(t) &= (\delta(t) + 1/b)/a, \\ k_2(t_1, t_2) &= -\delta(t_1)\delta(t_2)/2a. \end{aligned} \tag{15}$$

The relations for the cascade $\mathbf{G} = \mathbf{H} * \mathbf{K}$ are (Brilliant, 1958)

$$G_1(s) = H_1(s)K_1(s),$$
$$G_2(s_1, s_2) = H_1(s_1 + s_2)K_2(s_1, s_2) + H_2(s_1, s_2)K_1(s_1)K_1(s_2).$$

Thus

$$G_1(s) = (1 + 1/bs)H_1(s)/a,$$
$$G_2(s_1, s_2) = -H_1(s_1 + s_2)/2a + (1 + 1/bs_1)(1 + 1/bs_2)H_2(s_1, s_2)/a^2. \tag{16}$$

Transforming the latter expressions to the time domain gives

$$g_1(t) = \left(h_1(t) + \frac{1}{b}\int_0^t h_1(\rho)\,d\rho\right)\Big/a,$$
$$g_2(t_1, t_2) = \left(h_2(t_1, t_2) + \frac{1}{b}\left[\int_0^{t_2} h_2(t_1, \rho_2)\,d\rho_2 + \int_0^{t_1} h_2(\rho_1, t_2)\,d\rho_1\right]\right.$$
$$\left. + \frac{1}{b^2}\int_0^{t_1}\int_0^{t_2} h_2(\rho_1, \rho_2)\,d\rho_1\,d\rho_2\right)\Big/a^2 - h_1(t_1)\delta(t_2 - t_1)/2a. \tag{17}$$

In the actual computation of $g_2(t_1, t_2)$ the diagonal singularity in the last term was broadened with the substitution for $\delta(t_2 - t_1)$ of the normalized sampling function (Goldman, 1953) $\sin(2W\pi(t_2 - t_1))/\pi(t_2 - t_1)$. The value used for the bandwidth W was 1 min^{-1}, which is well beyond the cutoff frequency of *Phycomyces* (0.15 min^{-1}) and the white noise stimulus (0.30 min^{-1}). As such the sampling function has the same effect as the δ-function.

I wish to thank Prof. Max Delbrück for encouragement and for criticism of the manuscript and Prof. Gilbert McCann for generously providing his computer facilities. I am indebted to Dr. Panos Marmarelis and Dr. Ken Foster for valuable discussions and to Messrs. Bruce Elgin, Dale Knutsen, and Roque Szeto for assistance with computer software and hardware. I am grateful to Mr. Michael Walsh for excellent technical assistance and Mrs. Jeanette Navest for preparation of cultures.

This work was supported by grants from the National Science Foundation (BMS 70-00999 A04) and the National Institutes of Health (GM 21409) to Dr. M. Delbrück, and from the National Science Foundation (GJ 42025) and the National Institutes of Health (NS 03627) to Dr. G. D. McCann. The author held a postdoctoral fellowship (1 F02 GM 53785) from the National Institutes of Health.

Received for publication 18 February 1975.

REFERENCES

BARRETT, J. M. 1963. The use of functionals in the analysis of nonlinear physical systems. *J. Electron. Control.* **15**:567.

BERGMAN, K., P. V. BURKE, E. CERDÁ-OLMEDO, C. N. DAVID, M. DELBRÜCK, K. W. FOSTER, E. W. GOODELL, M. HEISENBERG, G. MEISSNER, M. ZALOKAR, D. S. DENNISON, and W. SHROPSHIRE, JR. 1969. *Phycomyces. Bacteriol. Rev.* **33**:99.

BERGMAN, K., A. P. ESLAVA, and E. CERDÁ-OLMEDO. 1973. Mutants of *Phycomyces* with abnormal phototropism. *Mol. Gen. Genet.* **123**:1.

BLACKMAN, R. B., and J. W. TUKEY. 1958. The Measurement of Power Spectra. Dover Publications, Inc., New York. 86.

BRILLIANT, M. B. 1958. Theory of the analysis of nonlinear systems. *Res. Lab. Electron. M.I.T. (Cambridge, Mass.) Tech. Rep. 345.*

COHEN, R. J. 1974. Cyclic AMP levels in *Phycomyces* during a response to light. *Nature (Lond.).* **251**:144.

COHEN, R. J., Y. N. JAN, J. MATRICON, and M. DELBRÜCK. 1975. The avoidance response, the house response, and the wind responses of the sporangiophore of *Phycomyces. J. Gen. Physiol.* **66**:67.

COLE, K. S. 1968. Membranes, Ions and Impulses. University of California Press, Berkeley.

COOLEY, J. W., and J. W. TUKEY. 1965. An algorithm for the machine calculation of complex Fourier series. *Math. Comput.* **19**:297.

DELBRÜCK, M., and W. REICHARDT. 1956. System analysis for the light growth reactions of *Phycomyces. In* Cellular Mechanisms in Differentiation and Growth. Dorothea Rudnick, editor. Princeton University Press, Princeton, N.J. 3–44.

DENNISON, D. S., and R. P. BOZOF. 1973. Phototropism and local adaptation in *Phycomyces* sporangiophores. *J. Gen. Physiol.* **62**:157.

EISENBERG, M., J. E. HALL, and C. A. MEAD. 1973. The nature of the voltage dependent conductance induced by alamethicin in black lipid films. *J. Membrane Biol.* **14**:143.

FOSTER, K. W. 1972. The photoresponses of *Phycomyces:* analysis using manual techniques and an automated machine which precisely tracks and measures growth during programmed stimuli. Ph.D. Thesis, California Institute of Technology, Pasadena.

FOSTER, K. W., and E. D. LIPSON. 1973. The light growth response of *Phycomyces. J. Gen. Physiol.* **62**: 590.

FRENCH, A. S., and E. G. BUTZ. 1973. Measuring the Wiener kernels of a non-linear system using the fast Fourier transform algorithm. *Int. J. Control.* **17**:529.

GOLDMAN, S. 1953. Information Theory. Dover Publications, Inc., N.Y.

HAMILTON, W. C. 1964. Statistics in Physical Science. Ronald Press, New York.

LEE, Y. W., and M. SCHETZEN. 1965. Measurement of the Wiener kernels of a nonlinear system by cross-correlation. *Int. J. Control.* **2**:237.

LIPSON, E. D. 1975 *a*. White noise analysis of *Phycomyces* light growth response system. II. Extended intensity ranges. *Biophys. J.* **15**:1013.

LIPSON, E. D. 1975 *b*. White noise analysis of *Phycomyces* light growth response system. III. Photomutants. *Biophys. J.* **15**:1033.

MARMARELIS, P. Z., and K.-I. NAKA. 1973. Nonlinear analysis and synthesis of receptive-field responses in the catfish retina. *J. Neurophysiol.* **36**:605.

MCCANN, G. D. 1973. Interactive computer strategies for living nervous system research. *IEEE Trans. Bio-Med. Eng.* BME-**20**:1.

MCCANN, G. D. 1974. Nonlinear identification theory models for successive stages of visual nervous systems of flies. *J. Neurophysiol.* **37**:869.

MILSUM, J. H. 1966. Biological Control Systems Analysis. McGraw-Hill Book Company, New York.

MÜLLER, P., and D. O. RUDIN. 1968. Action potentials induced in bimolecular lipid membranes. *Nature (Lond.).* **217**:713.

RUSHTON, W. A. H. 1965. Visual adaptation. *Proc. R. Soc. Lond. B Biol. Sci.* **162**:20.

WIENER, N. 1958. Nonlinear Problems in Random Theory. John Wiley & Sons, New York.